A Fully Verified Theoretical Analysis of Contact-Mode Triboelectric Nanogenerators as a Wearable Power Source

*Bao Yang, Wei Zeng, Ze-Hua Peng, Shi-Rui Liu, Ke Chen, and Xiao-Ming Tao**

Harvesting mechanical energy from human activities by triboelectric nanogenerators (TENGs) is an effective approach for sustainable, maintenance-free, and green power source for wireless, portable, and wearable electronics. A theoretical model for contact-mode triboelectric nanogenerators based on the principles of charge conservation and zero loop-voltage is illustrated. Explicit expressions for the output current, voltage, and power are presented for the TENGs with an external load of resistance. Experimental verification is conducted by using a laboratory-fabricated contact-mode TENG made from conducting fabric electrodes and polydimethylsiloxane/graphene oxide composite as the dielectric layer. Excellent agreements of the output voltage, current, and power are demonstrated between the theoretical and experimental results, without any adjustable parameters. The effects of the moving speed on output voltage, current, and power are illustrated in three cases, that is, the motion with constant speed, the sinusoidal motion cycles, and the real walking cycles by human subject. The fully verified theoretical model is a very powerful tool to guide the design of the device structure and selection of materials, and optimization of performance with respect to the application conditions of TENGs.

1. Introduction

Harvesting mechanical energy from human activities is an effective approach for sustainable, maintenance-free, and green power source for wireless, portable, and wearable electronics.[1–3] It is estimated that harvesting even 1%–5% of the body's power without significantly increasing the load to the human body will be sufficient to run many body-worn devices.[4,5] Triboelectric nanogenerators (TENGs) have been demonstrated to harvest energy from the human activities as sustainable self-sufficient micro/nano-power sources, due to their high efficiency, low cost, environmental friendliness, and universal availability.[6–18] To improve the performance and broaden the applications of TENGs, numerous efforts have been made with focus on both enhancement of the surface charge density and development of new structures/modes.[2,4,7,9,13,19–25] So far, the electric power output of TENGs has been improved up to ≈500 W m^{-2} by sophisticated design of device structure.[18,26–28] Demonstrated TENGs have been working in four modes, that is, the contact-separation or contact mode in short, sliding mode, single-electrode mode, and free-standing triboelectric-layer mode. The performance of the TENGs in contact-mode is better than that of TENGs in the sliding mode, because a much higher maximum displacement of TENGs in the sliding mode is required than that of TENGs working in the contact-mode, in order to achieve the same level of open circuit voltage.[29] The TENGs working in the contact-mode are particularly interesting for applications like foot-mounted wearable electronic systems because of the short vertical displacement involved and ease of integration.

The fundamental principle of TENGs is based on the coupled effects of triboelectrification and electrostatic induction. A theoretical model has been proposed for the TENGs working in the contact mode by Wang and co-workers. By utilizing the derived governing equation, the real-time output characteristics and the relationship between the optimum external resistance and TENG parameters were numerically simulated.[30] However, the model was not validated by corresponding experiments with measured real-time output characteristics. Furthermore, it is known that the real-time output characteristics would be affected by the materials, device structural parameters, operation conditions, and equivalent resistance. Assumptions made on simple profiles of working velocity may influence the model's validity in real situations. For instance, during real human walking, the previous wearing trials of an intelligent footwear system illustrated that the velocity profile was complex and varied significantly with time for a foot-mounted device.[31,32] Therefore, it is highly desirable to develop a theoretical model that is fully verified by corresponding experiments. Such an experimentally verified model is essential for designing and optimizing TENGs for intended applications.

In this paper, based on conservation of charges and zero-voltage for close-loop circuits, a theoretical model is presented

Dr. B. Yang, Dr. W. Zeng, Z.-H. Peng, S.-R. Liu, K. Chen, Prof. X.-M. Tao
Nanotechnology Center of Functional and Intelligent Textiles and Apparel
Institute of Textiles and Clothing
The Hong Kong Polytechnic University
Hong Hum, Kowloon, Hong Kong
E-mail: xiao-ming.tao@polyu.edu.hk

DOI: 10.1002/aenm.201600505

for the contact-mode TENG connected with an external resistor. Explicit expressions for the output current, voltage, and power are presented for the TENGs with an external load of resistance, which take full considerations of the materials, device structural parameters, and loading conditions. Corresponding experiments are performed to verify the theoretical model. Excellent agreements are demonstrated between the theoretical and experimental results. The output current, voltage, and power of the contact-mode TENGs are systematically investigated. A fabricated TENG connected with an external resistor of 60 MΩ is demonstrated possessing peak power density of 2.6 W m^{-2}.

2. Theoretical Treatment for Contact-Mode TENGs

In general, a contact-mode TENG works with a connected resistor R as shown in **Figure 1**. To illustrate the model, a dielectric-conductor TENG is used. The top electrode moves up and down with a separation distance, x, from a fixed dielectric layer, which is fixed on the bottom electrode.

Being forced to get in contact with each other, the contact surface of the top electrode and the dielectric layer will have opposite triboelectric charges of an equal areal density, as a result of contact electrification. After sufficient contact, the surface charges of the top electrode and the dielectric layer both will reach a saturation state. Considering the saturated surface charges, it is reasonable to assume that the tribocharges are uniformly distributed on the dielectric layer with negligible decay (denoted as surface charge density, σ, as shown in Figure 1).[1–3] When the two triboelectric layers start to separate from each other, with increasing x, the surface charge density of two electrodes are changed due to electrostatic induction, and the surface charge density of the two electrodes are denoted as σ_1 and σ_2, respectively, which satisfy the following charge conservation condition

$$\sigma_1 + \sigma_2 - \sigma \equiv 0 \tag{1}$$

The electric potentials of the close loop of the circuit in Figure 1 should satisfy the following condition

$$\sum_{i=1}^{N} V_i = 0 \tag{2}$$

where V_i represents the voltage of the ith part in the close loop of the circuit.

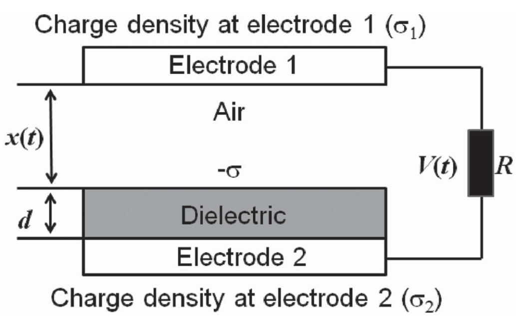

Figure 1. Schematic diagram of a conductor-to-dielectric contact-mode TENG connected with an external resistor.

Since the areal size (S) of the dielectric layer and electrodes is several orders of magnitude larger than its effective separation distance x and the thickness d of dielectric, respectively, the corresponding electric fields can be simply calculated by Gauss's law:-

Inside the air gap

$$E_a = -\frac{\sigma_1}{\varepsilon_0} \tag{3}$$

Inside the dielectric layer

$$E_d = -\frac{\sigma_2}{\varepsilon_0 \varepsilon_r} \tag{4}$$

where ε_0 and ε_r are denoted as the vacuum permittivity and the relative permittivity, respectively.

According to Equation (2), one can obtain

$$E_a x(t) + E_d d + V(t) = 0 \tag{5}$$

The amount of the transferred charges between the two electrodes is defined as Q, which also represents the amount of charges that go through the resistor. In the case that at $t = 0$, the two contacting layers are close to each other for a sufficiently long time so that the contact electrification reaches its saturation. Then the top electrode layer starts to separate from the dielectric layer. Initial conditions are given by

$$Q(t=0) = 0 \tag{6}$$

$$\sigma_2 = \frac{Q}{S} \tag{7}$$

As a power source in practical use, the TENG will be connected with an external load. Hence, in this situation, the real charge transfer rate will be limited by the external resistor, R. According to the Ohm's law, the output voltage V can be expressed as

$$V(t) = RI(t) = R\frac{dQ}{dt} \tag{8}$$

Merging Equations (1), (3)–(5), (7), and (8), one can have

$$R\frac{dQ}{dt} + \frac{Q}{S\varepsilon_0}(d_0 + x(t)) - \frac{\sigma x(t)}{\varepsilon_0} = 0 \tag{9}$$

where both parameters of the thickness d and the relative permittivity ε_r of the dielectric layer have been combined as the effective thickness constant d_0 ($d_0 = d/\varepsilon_r$).

By combining the initial conditions in Equation (6), differential Equation (9) can be solved analytically as follows

$$Q(t) = \left[\int_0^t \frac{\sigma x(\tau)}{R\varepsilon_0} e^{\int_0^\tau \frac{d_0 + x(z)}{RS\varepsilon_0} dz} d\tau\right] e^{-\int_0^t \frac{d_0 + x(\tau)}{RS\varepsilon_0} d\tau} \tag{10}$$

As a result, the output current, voltage across the resistor, and power are described by the following equations, respectively

Table 1. Simulation parameters utilized in the verification of theoretical model.

Symbol	Value
Total external resistance in the circuit R	10 [MΩ]
Areal size of the dielectric S	36 [cm^2]
Surface tribocharge density σ	15 [μC m^{-2}]
Thickness of dielectric layer d	250 [μm]
Relative permittivity of dielectric layer ε_r	3.4
Effective thickness of dielectric layer d_0	73.53 [μm]
Vacuum permittivity ε_0	8.854×10^{-12} [F m^{-1}]
Amplitude of the motion A_0	5 [mm]
Frequency f	3.2 [Hz]
Angular velocity ω	$2\pi f$ [rad s^{-1}]
Initial phase angle θ	$3\pi/2$ [rad]

$$I(t) = \frac{dQ}{dt} = \frac{\sigma x(t)}{R\varepsilon_0} - \frac{d_0 + x(t)}{RS\varepsilon_0} . e^{-\int_0^t \frac{d_0+x(\tau)}{RS\varepsilon_0} d\tau} . \int_0^t \frac{\sigma x(\tau)}{R\varepsilon_0} e^{\int_0^\tau \frac{d_0+x(z)}{RS\varepsilon_0} dz} d\tau \tag{11}$$

$$V(t) = RI(t) = \frac{\sigma x(t)}{\varepsilon_0} - \frac{d_0 + x(t)}{S\varepsilon_0} . e^{-\int_0^t \frac{d_0+x(\tau)}{RS\varepsilon_0} d\tau} . \int_0^t \frac{\sigma x(\tau)}{R\varepsilon_0} e^{\int_0^\tau \frac{d_0+x(z)}{RS\varepsilon_0} dz} d\tau \tag{12}$$

$$P(t) = \frac{[V(t)]^2}{R} = \frac{\left[\frac{\sigma x(t)}{\varepsilon_0} - \frac{d_0 + x(t)}{S\varepsilon_0} . e^{\int_0^t \frac{d_0+x(\tau)}{RS\varepsilon_0} d\tau} . \int_0^t \frac{\sigma x(\tau)}{R\varepsilon_0} e^{\int_0^\tau \frac{d_0+x(z)}{RS\varepsilon_0} dz} d\tau^2 \right]}{R} \tag{13}$$

It is noted that although the governing Equation (9) has a form identical to the previous model proposed by Niu et al.,[30] the explicit analytical solutions for voltage, current, and power, as expressed in Equations (10)–(13), are different in their mathematic forms.

A sinusoidal motion of the top electrode, described by Equation (14), was selected because the verifying experimental rig (Keyboard Life Tester by Shenzhen ZXD Testing Equipment Co. Ltd.) was equipped with this form of motion. A motion with constant speed was also considered. When $t = 0$, the two contact surfaces of the top electrode and the dielectric layer have experienced contact for a sufficiently long time so that the contact electrification reaches its saturation. Then the top electrode started to separate from the dielectric layer.

$$x(t) = A_0 \sin(\omega t + \theta) + A_0 \tag{14}$$

where A_0 and ω are the amplitude and the angle velocity of the motion, respectively. θ is the initial phase angle. The parameters utilized in the simulation corresponded to those used in the experiments, which are listed in **Table 1**.

3. Conclusions

In summary, we have proposed a theoretical model for contact-mode triboelectric nanogenerators. Explicit expressions for the output current, voltage, and power have been presented for a TENG with an external load of resistance. Experimental verification, by using a lab-fabricated contact-mode TENG made from conducting fabric electrodes and PDMS/GO composite as the dielectric layer, was conducted and reached an excellent agreement with the simulation results based on the theoretical models and real experimental conditions. The effects of moving speed on output voltage, current, and power were investigated in three cases, that is, the motion with constant speed, the sinusoidal moving cycles, and the real walking cycles by human subject. The fully verified theoretical model would be a very powerful tool to guide the design of the device structure and selection of materials for TENGs, and optimization of TENGs with respect to their application conditions.

4. Experimental Section

To validate the theoretical model derived, corresponding experiments were designed and carried out. The contact-mode TENG was made from a dielectric coating layer of polydimethylsiloxane/graphene oxide (PDMS/GO) composite as the electronegative material and a Cu/Ni coated conducting fabric (provided by 3M) as the electropositive material. **Figure 2**a illustrated the schematic diagram of the fabricated TENG, which had a double-layer structure including a PDMS/GO composite coating and a conducting fabric fixed on an acrylic plate, another conducting fabric fixed on the top moving acrylic plate. The top conducting fabric electrode played dual roles of electrode and contact surface. The composite coating layer played the role of dielectric. To effectively separate the two layers after contacting each other, four springs were installed at the corners, leaving a narrow space between the PDMS/GO coating and the top fabric electrode. A scanning electron microscopy (SEM) image of the conducting fabric was presented in Figure 2b,c. The conducting fabric had a woven structure with uniformly sized micropattern on the surface, which increased the effective contact area, thus enhancing the electrical output of TENG. PDMS was carefully chosen according to its electric affinity to attract electrons, and more importantly, the PDMS was easy for coating with high flexibility and durability. GO nanoparticles were embedded in PDMS matrix, the addition of GO in PDMS matrix might increase relative dielectric constant with a small loss factor. In the present study, the output voltage and current of as-fabricated TENG were much higher than that of the pure PDMS film based TENG. Furthermore, the dispersed GO in the PDMS acted as charge trapping sites, which increased the active interface for charge storage. Electrons attracted from PDMS through the friction process were stored either in the discrete, quantized levels of these nanosized graphene particles, or trapped in the amorphous GO dielectric. Both might result in a high surface charge density on the PDMS/GO composite, and low dissipation rate of surface charge.[33,34] Figure 2d displayed the surface structure of PDMS/GO coating, which revealed a smooth surface and uniformly dispersed GO nanoparticles in PDMS matrix. The cross-sectional view shown in Figure 2e revealed that the PDMS/GO coating was well deposited on the surface of the conducting fabric. To obtain the average thickness of the coating, the PDMS/GO coating layer was peeled off from the fabric for measurement at different positions by a spiral micrometer. The average thickness of PDMS/GO coating layer was obtained as ≈250 μm. A high resolution transmission electron microscopy (HRTEM) image of GO nanoparticles was presented in Figure 2f, and the lattice fringes were visible on the edges of GO sheets clearly.

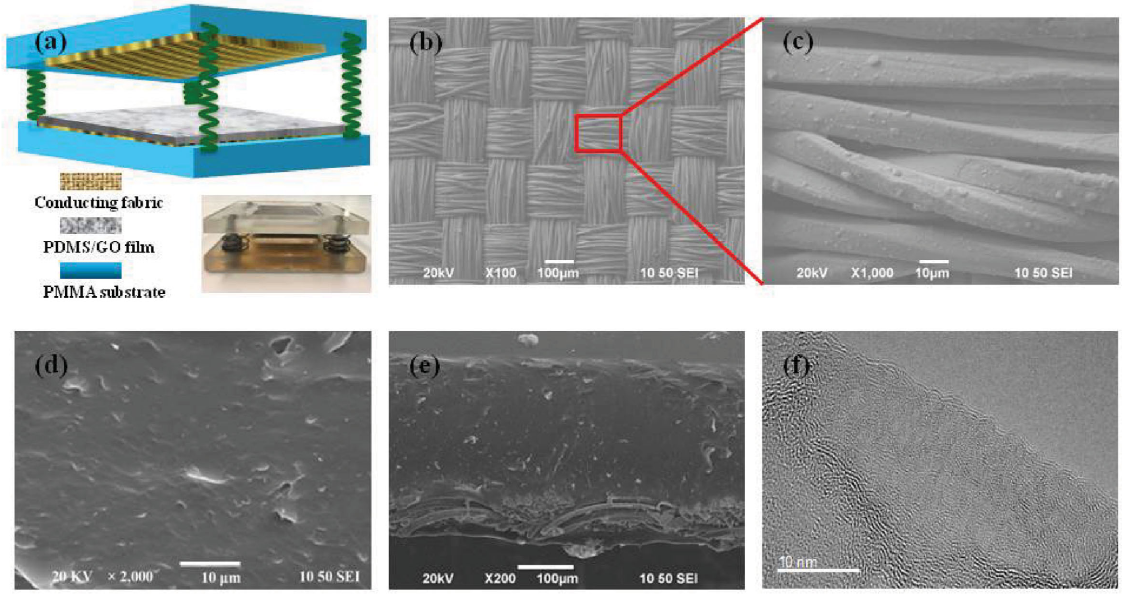

Figure 2. a) Schematic illustration and digital photograph of the TENG. b) SEM image of conducting fabric. c) Magnified image of (b). d) SEM images of the surface of PDMS/GO film. e) SEM image of the cross-section of the PDMS/GO coated conducting fabric. f) HRTEM image of GO.

The parameters of the contact mode TENG were given in Table 1. The surface charge density of the material was determined by using the Nanocoulomb Meter and Faraday tube (Models: 230, 232, and 234). The TENG samples were compressed by Keyboard Life Tester (ZXA-03) for a certain number of cycles, then the dielectric and electrodes were taken out for the measurements. The surface charges were collected by the Faraday tube and the number of charges was given by the Nanocoulomb Meter. The average value of surface density (surface charge per area) was derived from three tests. It was observed that the output voltage increased with increasing number of cycles, and at 500 cycles, it reached a stable saturation value. Thus the value of surface charge density was determined at 500 cycles.

The as-fabricated TENG was mechanically compressed repeatedly by a plate attached to a Keyboard Life Tester (ZX-A03), which provided a continuous dynamic sinusoidal motion with controlled levels of displacement from 0 to +10 mm and frequency from 1 to 5 Hz. It was equipped with a compression force cell so that the contact force was simultaneously measured. At the same time, the TENG was connected with an oscilloscope with an equivalent resistance of 10 MΩ. The contact electrification was a progressing process. It was observed that the surface charge density increased with contact length gradually and achieved a saturation state with equilibrium density. Thus the measurements of σ and the voltage of TENG were made after a cyclic compression about 500 times. Both the theoretical and measured voltages between two electrodes of the device were based on the saturated or equilibrium surface charge density.

Figure 3 showed the measured output voltage, current, and power of TENG during the compressive loading cycles. The TENG generated a positive and negative peak voltage of 40 and −35 V from the contacting and releasing action, respectively. Figure 3 also showed the simulation result based on Equations (11)–(13). The simulation parameters were listed in Table 1. Without any adjustment on simulation parameters,

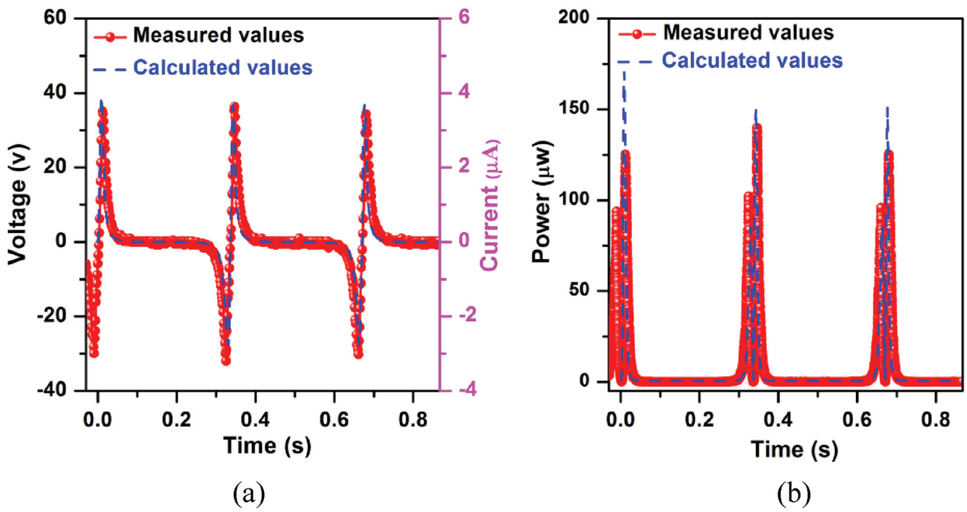

Figure 3. Comparison between the experimental and simulation results: a) Output voltage and current, b) Output power.

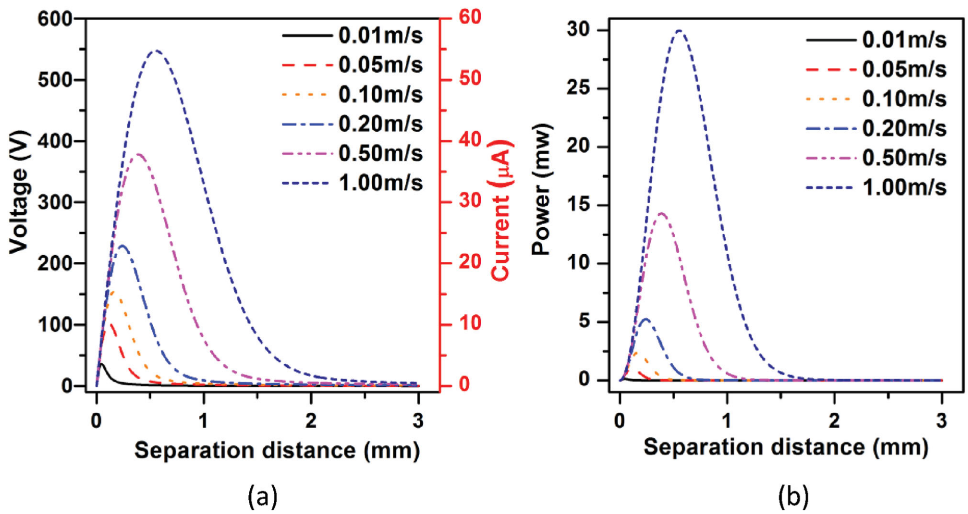

Figure 4. Calculated output characteristics for the first case of constant speed: a) Output voltage and current as functions of speed and separation distance, b) Output power as a function of speed and separation distance.

there was a strong agreement between the theoretical and experimental results, both the shape of the curve, locations of the peaks, and amplitudes of the data points in general.

The change of the spatial distance between the top electrode and the dielectric layer added the voltage difference between both the electrodes, while the flow of electrical charges diminished it. They were instantaneous and continuous processes. When the spatial displacement of the top electrode goes back to zero, the number of electrical charges did not return to its original value, which makes the next cycle behavior different from that of the initial one. Small discrepancies in amplitude appearing at the peaks showed that upon contacting, the first peak voltage was slightly higher than the next one.

According to Equations (11)–(13), the speed of the top plate of the TENG would also affect the output performance of the TENG. Therefore three cases were considered, including displacements with constant speed, sinusoidal displacement cycles with variation of frequency, and loading cycles of human foot falls. In the first case, numerical calculations were carried out with various levels of uniform speed and separation distances, as shown in **Figure 4**. The simulation parameters were given in **Table 2**. Figure 4a,b showed that the output voltage, current, and power of the TENG were increased monotonically with the increasing speed. Furthermore, the peak voltage arose with the increasing loading speed, the separation distance for the peak voltage shifted to a larger value. With a constant speed of 1 m s^{-1}, the maximum output voltage was ≈550 V and the peak power could be up to 30 mW when the separation distance was 0.75 mm.

Table 2. Simulation parameters utilized in the first case of constant speed.

Symbol	Value
Total external resistance in the circuit R	10 [MΩ]
Areal size of the dielectric S	36 [cm^2]
Surface tribo-charge density σ	15 [μC m^{-2}]
Thickness of dielectric layer d	250 [μm]
Relative permittivity of dielectric layer ε_r	3.4
Effective thickness of dielectric layer d_0	73.53 [μm]
Vacuum permittivity ε_0	8.854×10^{-12} [F m^{-1}]
Maximum separation distance x_{max}	3 [mm]
Releasing speed V	0.01–1.00 [m s^{-1}]

In the second case of sinusoidal displacement cycles, the frequency variation was considered as it could directly affect speed. A systematic measurement was performed under various values of frequency. As shown in **Figure 5**a, at 0.5 Hz, the peak output voltage generated by the TENG was 50 V. As the frequency increased from 0.5 to 2.5 Hz, the peak output voltage increased, and reached a maximum value of ≈100 V, with the same experimental setup for the verification experiments except the loading mode (Table 1). The enhancement in the electrical power generation by the increasing frequency could be explained by the higher speed of the top plate. Figure 5b,c depicted that the output voltage and current reached recorded values of 125 V and 12.5 μA, respectively, from the TENG under a peak external force (1000 N, equivalent to 278 KPa) of the pressing stage operating at a frequency of 3.2 Hz. Obviously, the TENG generated equivalent values of positive and negative voltage under the sinusoidal displacement cycles. The voltage curve with an obvious splitting in Figure 5c was due to the complex loading condition on the dielectric film. While the calculated values based on Equation (12) did not display any splitting because the pressure on the dielectric layer was assumed as zero. When an external force was applied on the dielectric layer, the thickness d of the dielectric film in equations was not a constant any more. And a new mechanism occured. When R was large, under a fast deformation period of dielectric film, the charge transfer was quite small. During such deformation period, the electric field, E_d, could be assumed to be constant. However the product, E_d d, had a fast change, which induced the output voltage changes. Hence, a large resistance and a fast deformation of dielectric layer led to an obvious splitting in the output voltage curves.

The stability of the TENG was an essential factor to ensure its practical applications. In the present study, the TENG was continuously operated for at least 1 000 000 cycles at a given frequency (3.2 Hz) and a peak compressive pressure of 278 KPa, which was chosen to be similar to the peak plantar pressure when a normal-weight person was walking.[31] As shown in Figure 5d, the generated output voltage of 125 V did not show any degradation after 1 000 000 cycles, indicating the highly stable power generation of the TENG, and this excellent durability makes the TENG advantageous as a sustainable power source for foot-mounted wearable electronic devices. This feature might be attributed to the robustness of the device, as no noticeable surface morphology degradation was detected in the PDMS/GO coating and conducting fabric.

In the third case of real walking cycles, a TENG was placed on the floor, a human subject of ≈50 kg continuously stepped on and off it with a foot. **Figure 6**a presented the output voltage and current of the TENG with the same conditions as those for the verification experiments listed

FULL PAPER

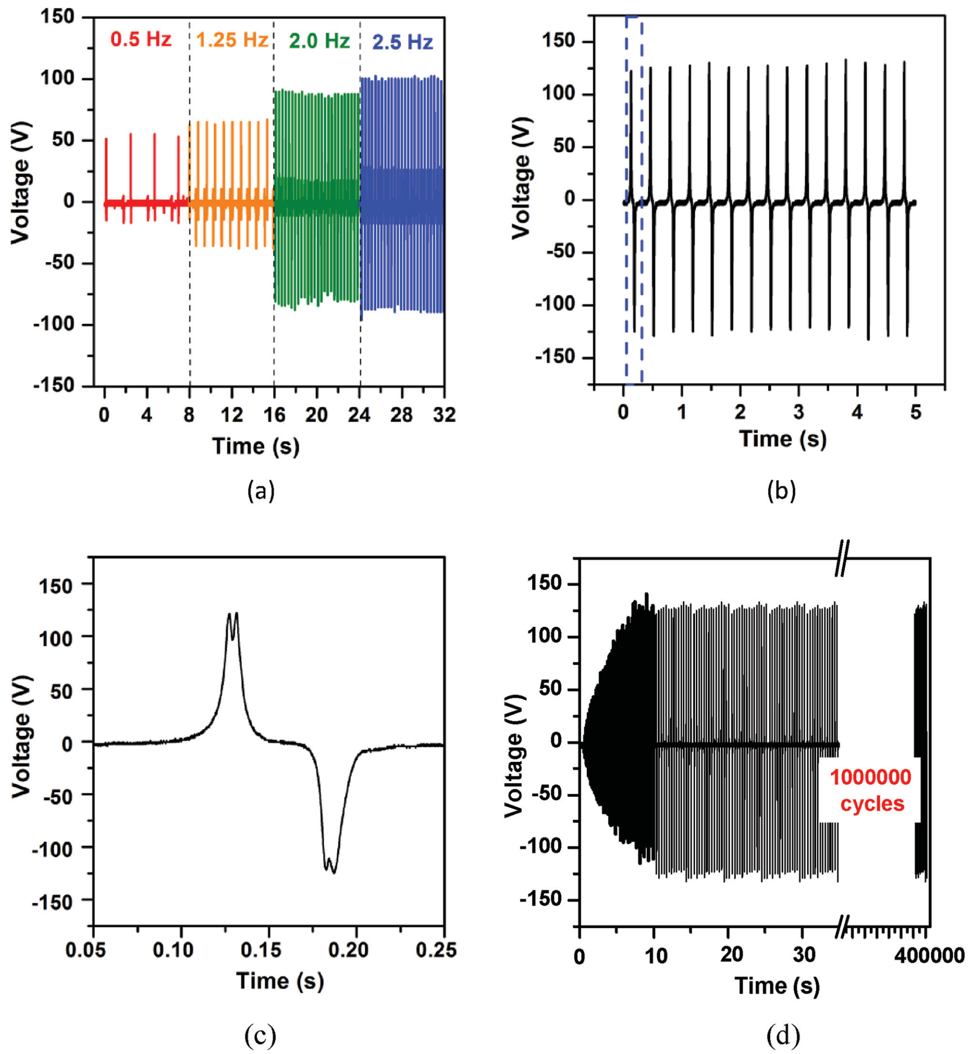

Figure 5. Frequency dependency of the output voltage of TENG: a) Frequency from 0.5 to 2.5 Hz, b) Frequency of 3.2 Hz, c) Enlarged section of (b), d) Cyclic compression up to 1 000 000 cycles with 3.2 Hz and 278 KPa peak pressure.

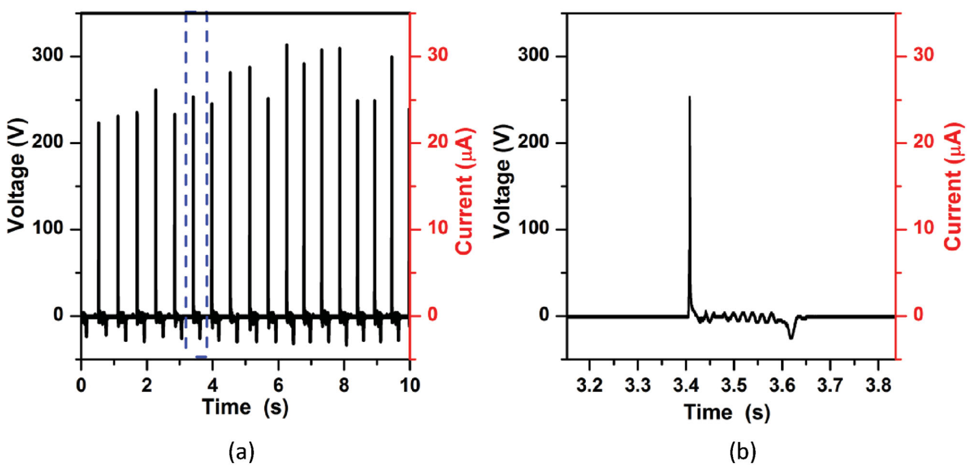

Figure 6. a) Measured output voltage and current of the TENG in the third case of human walking. b) Enlarged curve of (a).

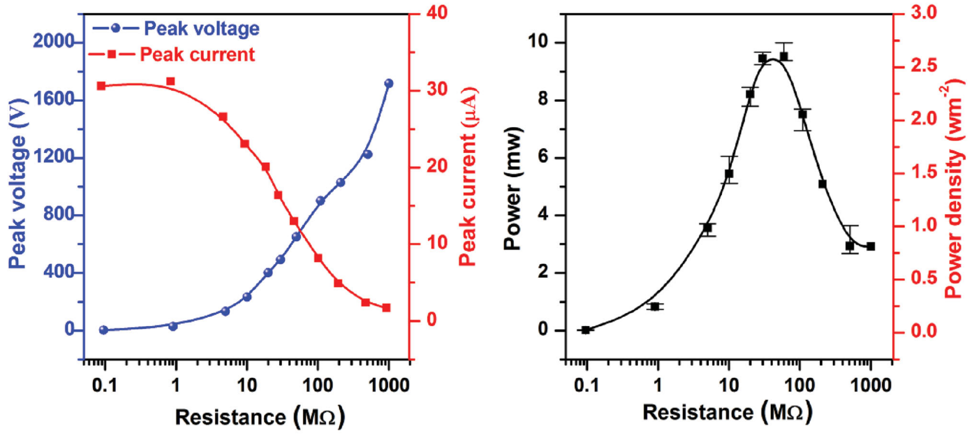

(a) (b)

Figure 7. Measurement results of the TENG (3.2 Hz and 278 KPa). a) Dependency of the voltage and the current on resistance. b) Dependency of the power and power density on the resistance.

in Table 1, except the loading mode. The TENG repeatedly generated a peak-to-peak positive voltage of 250 V and current reaches 25.0 μA. Figure 6b clearly showed that, in the separation phase, the negative peak output voltage (−25 V) and current (2.5 μA) of the TENG were one tenth of the positive values. The asymmetric peak shape of the generated voltage should be due to the nonuniform motion speed of footfall, which would deduce the different charge transfer rates between two electrodes. Figure 4 indicated that the output voltage was affected by the moving speed of the top electrode. Under the real condition of the human footfall during walking, the compression speed was much higher than that of the release speed,[31] thus the output negative output voltage of TENG was much smaller than that of positive output voltage.

The output voltage, current, power, and areal power density were determined experimentally as functions of external resistance, as summarized in **Figure 7**. They were measured at 3.2 Hz and with a peak compressive pressure of 278 KPa by using the Keyboard Life Time Tester. Figure 7a showed the peak current decreased with increasing resistance, while the voltage peak across the resistor exhibited a reversed tendency. Accordingly, the power and power density of the TENG first rose at low resistance region and then declined at high resistance, showing a maximum value of ≈2.6 W m^{-2} at the resistance load of 60 MΩ (Figure 7b).

The TENG was capable of instantaneously driving 150 commercial LEDs in a discontinuous manner. After rectifying, a commercial capacitor of 100 μF was used to store the energy from the TENG and to convent it in a more stable and continuous form. The output electric signals were first rectified by a bridge rectifier (inset in **Figure 8**a), transforming the alternating current to direct current (red curve in Figure 8a) and charging the capacitor continuously. The voltage across the capacitor was monitored during the charging process, and the charging curve of the capacitor was shown in Figure 8b. The capacitor was charged to 4 V after 1025 displacement cycles by Keyboard Life Tester at a frequency of 3.2 Hz.

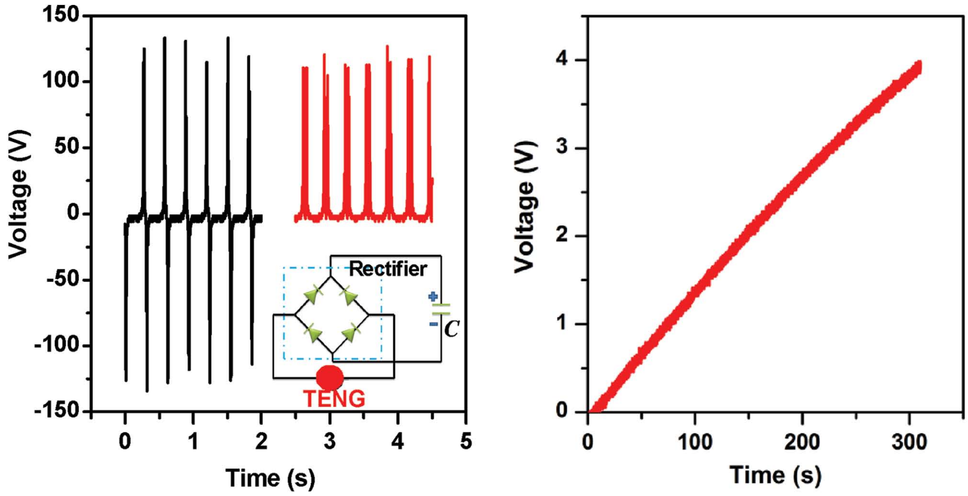

(a) (b)

Figure 8. a) Rectifying circuit and output voltage of a TENG (3.2 Hz and 278 KPa). b) Charging curve of a capacitor connected to TENG with the rectifying circuit.

Acknowledgements

The authors acknowledge the funding support from Research Grants Council of Hong Kong SAR Government (Project No. PolyU5272/11E, PolyU5251/13E, and PolyU152152/14E).

Received: March 4, 2016
Revised: April 22, 2016
Published online: June 14, 2016

[1] Z. L. Wang, W. Z. Wu, *Angew. Chem., Int. Ed.* **2012**, *51*, 11700.
[2] N. Y. Cui, J. M. Liu, L. Gu, S. Bai, X. B. Chen, Y. Qin, *ACS Appl. Mater. Interfaces* **2015**, *7*, 18225.
[3] W. Zeng, L. Shu, Q. Li, S. Chen, F. Wang, X. M. Tao, *Adv. Mater.* **2014**, *26*, 5310.
[4] W. Zhong, Y. Zhang, Q. Z. Zhong, Q. Y. Hu, B. Hu, Z. L. Wang, J. Zhou, *ACS Nano* **2014**, *8*, 6273.
[5] R. Riemer, A. Shapiro, *J. Neuroeng. Rehabil.* **2011**, *8*, 1.
[6] Z. L. Wang, G. Zhu, Y. Yang, S. H. Wang, C. F. Pan, *Mater. Today* **2012**, *15*, 532.
[7] X. F. Wang, S. M. Niu, Y. J. Yin, F. Yi, Z. You, Z. L. Wang, *Adv. Energy Mater.* **2015**, *5*, 1501467.
[8] J. Wang, X. H. Li, Y. L. Zi, S. H. Wang, Z. L. Li, L. Zheng, F. Yi, S. M. Li, Z. L. Wang, *Adv. Mater.* **2015**, *27*, 4830.
[9] F. Yi, L. Lin, S. M. Niu, P. K. Yang, Z. N. Wang, J. Chen, Y. S. Zhou, Y. L. Zi, J. Wang, Q. L. Liao, Y. Zhang, Z. L. Wang, *Adv. Funct. Mater.* **2015**, *25*, 3688.
[10] H. J. Fang, Q. Li, W. H. He, J. Li, Q. T. Xue, C. Xu, L. J. Zhang, T. L. Ren, G. F. Dong, H. L. W. Chan, J. Y. Dai, Q. F. Yan, *Nanoscale* **2015**, *7*, 17306.
[11] X. Y. Wei, G. Zhu, Z. L. Wang, *Nano Energy* **2014**, *10*, 83.
[12] T. Zhou, C. Zhang, C. B. Han, F. R. Fan, W. Tang, Z. L. Wang, *ACS. Appl. Mater. Interfaces* **2014**, *6*, 14695.
[13] W. Zeng, X. M. Tao, S. Chen, S. M. Shang, L. W. H. Chan, S. H. Choy, *Energy Environ. Sci.* **2013**, *6*, 2631.
[14] K. Y. Lee, J. Chun, J. H. Lee, K. N. Kim, N. R. Kang, J. Y. Kim, M. H. Kim, K. S. Shin, M. K. Gupta, J. M. Baik, S. W. Kim, *Adv. Mater.* **2014**, *26*, 5037.
[15] L. Lin, S. H. Wang, Z. L. Wang, *Abstr. Pap. Am. Chem. Soc.* **2014**, *247*, 452–ENVR.
[16] X. S. Zhang, M. D. Han, R. X. Wang, B. Meng, F. Y. Zhu, X. M. Sun, W. Hu, W. Wang, Z. H. Li, H. X. Zhang, *Nano Energy* **2014**, *4*, 123.
[17] H. L. Zhang, Y. Yang, Y. J. Su, J. Chen, K. Adams, S. Lee, C. G. Hu, Z. L. Wang, *Adv. Funct. Mater.* **2014**, *24*, 1401.
[18] G. Zhu, Z. H. Lin, Q. S. Jing, P. Bai, C. F. Pan, Y. Yang, Y. S. Zhou, Z. L. Wang, *Nano Lett.* **2013**, *13*, 847.
[19] X. D. Zhong, Y. Yang, X. Wang, Z. L. Wang, *Nano Energy* **2015**, *13*, 771.
[20] L. Zhang, L. Jin, B. B. Zhang, W. L. Deng, H. Pan, J. F. Tang, M. H. Zhu, W. Q. Yang, *Nano Energy* **2015**, *16*, 516.
[21] K. Zhang, X. Wang, Y. Yang, Z. L. Wang, *ACS Nano* **2015**, *9*, 3521.
[22] C. Y. Xue, J. Y. Li, Q. Zhang, Z. B. Zhang, Z. Y. Hai, L. B. Gao, R. T. Feng, J. Tang, J. Liu, W. D. Zhang, D. Sun, *J. Nanomater.* **2014**, *5*, 36.
[23] T. Quan, X. Wang, Z. L. Wang, Y. Yang, *ACS Nano* **2015**, *9*, 12301.
[24] G. L. Liu, W. N. Xu, X. N. Xia, H. F. Shi, C. G. Hu, *J. Mater. Chem. A* **2015**, *3*, 21133.
[25] T. Jiang, L. M. Zhang, X. Y. Chen, C. B. Han, W. Tang, C. Zhang, L. Xu, Z. L. Wang, *ACS Nano* **2015**, *9*, 12562.
[26] L. Lin, S. H. Wang, Y. N. Xie, Q. S. Jing, S. M. Niu, Y. F. Hu, Z. L. Wang, *Nano Lett.* **2013**, *13*, 2916.
[27] G. Zhu, J. Chen, T. J. Zhang, Q. S. Jing, Z. L. Wang, *Nat. Commun.* **2014**, *5*, 3426.
[28] G. Zhu, Y. S. Zhou, P. Bai, X. S. Meng, Q. S. Jing, J. Chen, Z. L. Wang, *Adv. Mater.* **2014**, *26*, 3788.
[29] Y. Zi, S. Niu, J. Wang, Z. Wen, W. Tang, Z. L. Wang, *Nat. Commun.* **2015**, *6*, 8376.
[30] S. M. Niu, S. H. Wang, L. Lin, Y. Liu, Y. S. Zhou, Y. F. Hu, Z. L. Wang, *Energy Environ. Sci.* **2013**, *6*, 3576.
[31] L. Shu, T. Hua, Y. Y. Wang, Q. A. Li, D. D. Feng, X. M. Tao, *IEEE Trans. Inf. Technol. Biomed.* **2010**, *14*, 767.
[32] L. Shu, X. M. Tao, D. D. Feng, *IEEE Sens. J.* **2015**, *15*, 442.
[33] J. Chen, H. Guo, X. He, G. Liu, Y. Xi, H. Shi, C. Hu, *ACS Appl. Mater. Interfaces* **2016**, *8*, 736.
[34] X. He, H. Guo, X. Yue, J. Gao, Y. Xi, C. Hu, *Nanoscale* **2015**, *7*, 1896.

